



UNIVERSITÀ
DEGLI STUDI
FIRENZE

FLORE

Repository istituzionale dell'Università degli Studi di Firenze

CO₂ and Rn degassing from the natural analog of Campo de Calatrava (Spain): Implications for monitoring of CO₂ storage sites

Questa è la Versione finale referata (Post print/Accepted manuscript) della seguente pubblicazione:

Original Citation:

CO₂ and Rn degassing from the natural analog of Campo de Calatrava (Spain): Implications for monitoring of CO₂ storage sites / Orlando Vaselli. - In: INTERNATIONAL JOURNAL OF GREENHOUSE GAS CONTROL. - ISSN 1878-0148. - ELETTRONICO. - 32:(2015), pp. 1-14. [10.1016/j.ijggc.2014.10.014]

Availability:

The webpage <https://hdl.handle.net/2158/1231499> of the repository was last updated on 2021-03-24T15:15:12Z

Published version:

DOI: 10.1016/j.ijggc.2014.10.014

Terms of use:

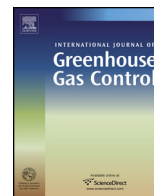
Open Access

La pubblicazione è resa disponibile sotto le norme e i termini della licenza di deposito, secondo quanto stabilito dalla Policy per l'accesso aperto dell'Università degli Studi di Firenze (<https://www.sba.unifi.it/upload/policy-oa-2016-1.pdf>)

Publisher copyright claim:

La data sopra indicata si riferisce all'ultimo aggiornamento della scheda del Repository FloRe - The above-mentioned date refers to the last update of the record in the Institutional Repository FloRe

(Article begins on next page)



CO₂ and Rn degassing from the natural analog of Campo de Calatrava (Spain): Implications for monitoring of CO₂ storage sites



J. Elío^{a,*}, M.F. Ortega^a, B. Nisi^b, L.F. Mazadiego^a, O. Vaselli^{c,d}, J. Caballero^a, F. Grandia^e

^a Universidad Politécnica de Madrid (UPM), Madrid, Spain

^b CNR-IGG Institute of Geosciences and Earth Resources, Pisa, Italy

^c Department of Earth Sciences, Florence, Italy

^d CNR-IGG Institute of Geosciences and Earth Resources, Florence, Italy

^e AMPHOS21, Barcelona, Spain

ARTICLE INFO

Article history:

Received 8 July 2014

Received in revised form 17 October 2014

Accepted 23 October 2014

Available online 13 November 2014

Keywords:

CO₂ storage

Geochemical monitoring

CO₂ leakages

Radon isotopes

Natural analogs

Soil gases

ABSTRACT

Natural analogs offer a valuable opportunity to investigate the long-term impacts associated with the potential leakage in geological storage of CO₂.

Degassing of CO₂ and radon isotopes (²²²Rn–²²⁰Rn) from soil, gas vents and thermal water discharges was investigated in the natural analog of Campo de Calatrava Volcanic Field (CCVF; Central Spain) to determine the CO₂–Rn relationships and to assess the role of CO₂ as carrier gas for radon. Furthermore, radon measurements to discriminate between shallow and deep gas sources were evaluated under the perspective of their applicability in monitoring programs of carbon storage projects.

CO₂ flux as high as 5000 g m^{−2} d^{−1} and ²²²Rn activities up to 430 kBq m^{−3} were measured; ²²⁰Rn activities were one order of magnitude lower than those of ²²²Rn. The ²²²Rn/²²⁰Rn ratios were used to constrain the source of the Campo de Calatrava soil gases since a positive correlation between radon isotopic ratios and CO₂ fluxes was observed. Thus, in agreement with previous studies, our results indicate a deep mantle-related origin of CO₂ for both free and soil gases, suggesting that carbon dioxide is an efficient carrier for Rn. Furthermore, it was ascertained that the increase of ²²²Rn in the soil gases was likely produced by two main processes: (i) direct transport by a carrier gas, i.e., CO₂ and (ii) generation at shallow level due to the presence of relatively high concentrations of dissolved U and Ra in the thermal aquifer of Campo de Calatrava.

The diffuse CO₂ soil flux and radon isotopic surveys carried out in the Campo de Calatrava Volcanic Fields can also be applicable to geochemical monitoring programs in CCS (Carbon Capture and Storage) areas as these parameters are useful to: (i) constrain CO₂ leakages once detected and (ii) monitor both the evolution of the leakages and the effectiveness of subsequent remediation activities. These measurements can also conveniently be used to detect diffuse leakages.

© 2014 Elsevier Ltd. All rights reserved.

1. Introduction

Carbon Capture and Storage (CCS) is one of the most feasible techniques to reduce anthropogenic greenhouse gas emissions into the atmosphere, allowing fossil fuels combustion to be environmentally sustainable (IEA, 2008; IPCC, 2005). In 2011 the United Nations Framework Convention on Climate Change of Durban (UNFCCC, 2011) defined CCS as a clean development mechanism. However, its commercial application still requires further (theoretical and practical) investigations in order to make this technology

economically viable and environmentally safe. Moreover, a proper evaluation of the costs (Kühn et al., 2013; Lupion and Herzog, 2013; Nataly Echevarria Huaman and Xiu Jun, 2014; Romanak et al., 2013) is needed since CCS can be difficult to sustain by private companies without financial support by governmental authorities unless carbon sequestration with enhanced gas recovery and oil recovery is applied (CSEGR and CSEOR; e.g., Oldenburg, 2003; Solomon et al., 2008). Eventually, as recently suggested, e.g., Oldenburg, 2012 and references therein, anthropogenic CO₂ can be used to improve the economic viability by increasing the use of this greenhouse gas for different (e.g., industrial, agricultural, food and beverages, pharmaceutical, chemical, healthcare) purposes. Thus, it has been suggested to include the term of “utilization of CO₂” in the CCS process, i.e., carbon capture, utilization and storage (CCUS).

* Corresponding author. Tel.: +34 91 3366 989; fax: +34 913 366 948.
E-mail address: javiereiliomedina@gmail.com (J. Elío).

The study of natural systems hosting CO₂-rich gas reservoirs can help to interpret the different stages of the CO₂ storage processes, which normally require long periods of time and can only partially be reproduced in the laboratory (Pearce, 2006). Consequently, in the recent years a large number of studies addressed to the evaluation of leakage processes from CO₂-rich natural analogs and the implications for the geological storage of CO₂ has been performed (e.g., Gal et al., 2012; Holloway et al., 2007; Jeandel et al., 2010; Lewicki et al., 2007; Voltattorni et al., 2009).

Surface monitoring methods (e.g., water and dissolved gas chemistry and soil-gas investigations) are relevant in the monitoring, verification and accounting (MVA) of CO₂ geosequestration to assess the environmentally safe storage (Klusman, 2011), during both site characterization and injection and post-injection phases. These methods have been oriented to detect and quantify possible CO₂ leakages to the atmosphere and cover a large range of techniques (e.g., IPPC, 2006; NETL, 2009).

Measurements of radon activity (²²²Rn–²²⁰Rn) in soil gases are considered useful in monitoring programs of geological storage for two main reasons: (i) CO₂ is often regarded as the main carrier gas for radon (e.g., Etiope and Martinelli, 2002; Etiope et al., 2005; Voltattorni et al., 2009), and then CO₂ leakages from deep sources may produce significant anomalies in radon activity, and (ii) radon, similarly to CO₂, can be used to detect fracture/fault systems since they represent the preferential pathways for gas leakage (e.g., Ioannides et al., 2003; Walia et al., 2010). Radon measurements at the soil-atmosphere interface for leakage detection were applied in some projects of CO₂ geological storage, such as the IEA GHG Weyburn CO₂ Monitoring and Storage Project (Riding and Rochelle, 2005; Strutt et al., 2003; Wilson and Monea, 2004) and the Frio Brine Pilot Project (Nance et al., 2005).

The detection of radon emission is also significant in terms of its effect on human health. USEPA has estimated that radon is the second cause of lung cancer after smoking (e.g., EPA, 2003; Field et al., 2000; Rosario and Wichmann, 2006). Thus, recognizing positive correlations between Rn and CO₂ and defining Rn abundances from permeable zones are critical and would allow the definition of potential hazard areas to be taken into consideration in the risk assessment of geological storage.

This research article describes and discusses the results obtained on free- and soil-gases from the Campo de Calatrava Volcanic Field (CCVF) natural analog, which is located in the Neogene Granátula – Moral de Calatrava Basin (central Spain). The main goals of this study were to (i) determine the relationships between CO₂ fluxes and activity of radon isotopes (²²²Rn and ²²⁰Rn) in the soil gas and (ii) to assess the possible use of radon measurements as monitoring tool in CCS projects.

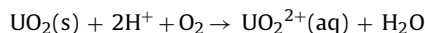
1.1. Radon physical-chemical background

Radon has four main isotopes, ²¹⁸Rn, ²¹⁹Rn, ²²⁰Rn and ²²²Rn, which are decay products of ²¹⁸At, ²²³Ra, ²²⁴Ra and ²²⁶Ra, respectively, all belonging to the U and Th decay series. Radon isotopes are characterized by relatively short half-lives being ²²²Rn ($t_{1/2} = 3.8$ days) and ²²⁰Rn ($t_{1/2} = 55$ seconds) with the longest half-lives (e.g., Fleischer, 1997). The decay products of ²²⁰Rn (commonly named thoron) and ²²²Rn are the radioactive isotopes of polonium, bismuth, lead and thallium. While ²²⁰Rn has no long-lived progeny, ²²²Rn has ²¹⁴Pb, ²¹⁴Bi and ²¹⁴Po (e.g., Ramachandran and Sathish, 2011).

Radon (²²²Rn–²²⁰Rn) activity has extensively been used in the earth sciences as tracer of U deposits (e.g., Sutton and Soonwala, 1975), precursor of seismic and volcanic activity (e.g., Cox, 1980; Dueñas and Fernández, 1987; Fleischer and Mogro-Campero, 1978; Nielson, 1978), tracer of subsurface fracture systems (Walia et al., 2010), oil/gas reservoirs (Klusman and Voorhees, 1983; Morse et al.,

1982; Mazadiego, 1994) and subsurface hydrocarbon pollution (Davis et al., 2003; García-González et al., 2008; Schubert et al., 2001). Recently, radon isotopes have been applied to distinguish CO₂ emission from deep and shallow (biogenic) sources (Etiope et al., 2005; Etiope and Martinelli, 2002; Giammanco et al., 2007; Michel-Le Pierres et al., 2010; Voltattorni et al., 2009).

A schematic cycle of ²²⁰Rn and ²²²Rn isotopes is reported in Fig. 1. The mobility of radon isotope parents, including uranium and radium, is limited. Uranium (an element with long-lived isotopes) is found in minerals and chemical alteration favors its transfer to surface and ground waters (e.g., Bonotto and Andrews, 1999; Mazadiego, 1994). Aqueous dissolution of uranium minerals (e.g., uraninite) can be represented by the following reaction:



Additionally, if water contains HCO₃[−] and CO₃^{2−} the mobility of uranium tends to increase due to the formation of carbonate complexes (Casas et al., 1998; Gorman-Lewis et al., 2008; Majumdar et al., 2003). Under oxidizing conditions, uranium in solution is preferentially present as uranyl ion (UO₂²⁺), whereas U⁴⁺ prevails in reducing conditions and UO₂ can precipitate (e.g., Bonotto and Andrews, 1999; García-González et al., 2008).

The uranyl ion may also be trapped in clay minerals and iron oxy-hydroxides by adsorption/absorption processes (e.g., Hsi and Langmuir, 1985; Langmuir, 1978). Conversely, radium (with shorter-lived isotopes than uranium) is exclusively present in solution as Ra²⁺ (Langmuir and Riese, 1985) and is rather recalcitrant to form salts under reducing and oxidizing environments. Thus, in surface and ground waters radium is maintained in solution. Neutral or anionic (e.g., SO₄) complexes are formed for pH approaching 10 (Langmuir and Riese, 1985). Nevertheless, according to Langmuir and Melchoir (1985) and Martin and Akber (1999), Ra²⁺ can coprecipitate with barite (BaSO₄), witherite (BaCO₃) and celestite (SrSO₄). Consequently, spring waters and related salts may represent a source of radon (²²²Rn–²²⁰Rn), whose values can be higher than those of the background signals.

In the vadose zone, Rn may also have a deep origin although, due to its relatively fast decay, radon is expected to have small mobility from its source by diffusion processes (Cothorn and Smith, 1987; Martinelli, 1998; Rose et al., 1979). Thus, underground long migration of radon from deeper sources to the surface requires advective transport driven by major gases such as CO₂ and CH₄ (the “geogas” theory, Etiope and Martinelli, 2002).

As Rn migrates, the radon isotopic ratios change due to significant differences in the ²²²Rn and ²²⁰Rn half-lives. The latter is thus preferentially found close to the parent isotope source (Huxol et al., 2012, 2013). The ²²²Rn/²²⁰Rn ratios can be used to define the depth at which free- and soil-gases retrieved at the surface were formed (e.g., Giammanco et al., 2007). The relationship between ²²²Rn and ²²⁰Rn in soil gases is clearly dependent on the concentration of their parents in the substrate (²³⁸U and ²³²Th, respectively). Thus, leaking of deep-seated gases at the surface is expected to result in reduced ²²⁰Rn concentrations, while the ²²²Rn/²²⁰Rn ratios increase. Relatively low ²²²Rn/²²⁰Rn ratios are generally associated with the production of radon in shallow environments (e.g., Giammanco et al., 2007).

Radon concentrations in soil gases are affected by a number of factors, such as meteorological, geological and pedological (e.g., De Jong et al., 1994; Vaupotic et al., 2007) and major seismic events (e.g., King and Minissale, 1994; Toutain and Baubron, 1999; Virk and Walia, 2001). According to Tanner (1980), radon can be released from soils and rocks by molecular diffusion, direct recoil and molecular diffusion after indirect recoil. Molecular and convection processes influence soil radon activity concentrations, which

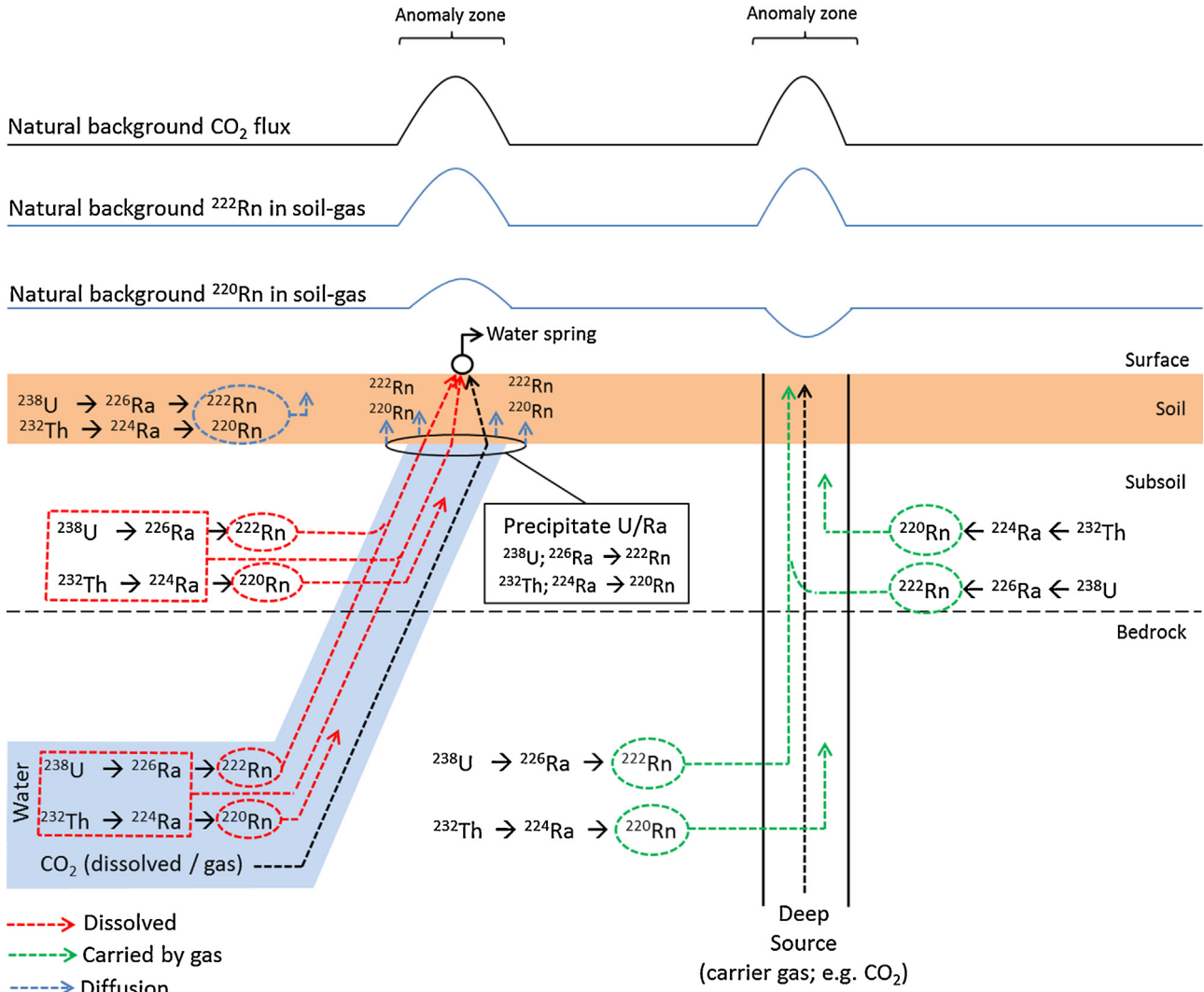


Fig. 1. Sketch of radon transport in liquid and gas phase.

increase with depth until when an equilibrium concentration is achieved (Nazaroff and Nero, 1988; Szabó et al., 2013).

Radon (^{222}Rn) concentration (C_{Rn} in $[\text{Bq m}^{-3}]$) in soil gases depends on ^{226}Ra concentration (C_{Ra} $[\text{Bq kg}^{-1}]$), emanation coefficient (ε ; adimensional), soil density (ρ $[\text{kg m}^{-3}]$) and effective porosity (n ; adimensional) (Guerra and Lombardi, 2001; Schubert et al., 2001), as follows:

$$C_{\text{Rn}} = C_{\text{Ra}} \cdot \varepsilon \cdot \rho \cdot n^{-1} \quad (1)$$

Soil water (saturation in pore space, $0 \leq S_F \leq 1$) increases radon concentration in soil gas (Schubert et al., 2001). Such an increase is defined by Eq. (2) ($K_{\text{w/air}} = 0.25$, radon partitioning coefficients between water and air) and plotted in Fig. 2. It can be seen that the ^{222}Rn concentration can increase up to 300% ($S_F = 1$) with respect to radon equilibrium in dry soil ($S_F = 0$).

$$\frac{1}{1 - S_F + S_F \cdot K_{\text{w/air}}} \quad (2)$$

2. Geological outlines

The Campo de Calatrava Volcanic Field (CCVF) is located in the province of Ciudad Real (central Spain) (Ancochea, 1983; Hernández-Pacheco, 1932; Fig. 3a). The study area consists of a

Hercynian basement covered by late Cenozoic sediments. This basement is unconformably overlain by upper Miocene to Quaternary fluvial and lacustrine sediments deposited within a series of fault-bounded Tertiary-Quaternary sedimentary basins of up to 200 km². A complex fracture pattern (E–W to ENE–WSW, NW–SE and NE–SW) controls the basins geometries (Crespo, 1992). At least three different Neogene tectonic episodes were recognized in the CCVF (IGME, 1988). A first extensional phase of late Miocene age, which resulted in the initial opening of the sedimentary basins, was followed in time by two Pliocene tectonic episodes: the opening of the so-called La Mancha basin and a final regional-scale weak compressional phase. The Miocene-Quaternary CCVF consists of volcanic deposits of alkaline composition (e.g., Cebriá et al., 2009; Cebriá and López-Ruiz, 1995; López-Ruiz et al., 2002). The area is characterized by several gas and water discharges (e.g., Melero Cabañas, 2007; Piedrabuena, 1992; Vaselli et al., 2013) that are distributed almost throughout the whole CCVF. It is interesting to point out that the geochemical and isotopic features of the gas seeps indicate a high purity of CO₂ (up to 98.5% by vol.), while the helium isotopic ratio suggests a mantle-related source for these gases (Pérez et al., 1996; Vaselli et al., 2013). The CCVF, along with La Selva-Empordà (NE Spain), likely represents the highest CO₂ discharge area in the whole continental Spain (Vaselli et al., 2013).

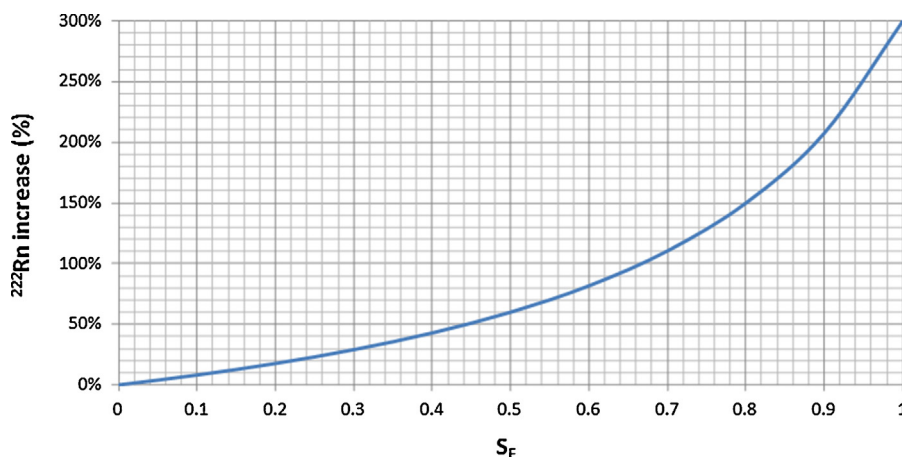


Fig. 2. Water influence in the equilibrium radon (^{222}Rn) concentration of the soil-gas.

3. Materials and methods

3.1. Area of study

More than 25 CO_2 seepages from CCVF, mainly associated to fracture systems, were investigated from June 2010 to February 2012. Gas leakages were commonly found as small ($<1 \text{ m}^2$) leakage points. Considering the elevated number of CO_2 emissions, this study focused on two areas that were considered representative of the CO_2 seepage in CCVF, namely La Sima (dry gas vents) and Jabalón River (degassing pools and springs) (Fig. 3a).

La Sima is a CO_2 -rich gas discharge (up to 2 t d^{-1}), which has a surface of a few square meters. The emission is restricted to a small ($\approx 5 \text{ m}$ in diameter) depression, where small dead animals are frequently found. The Jabalón River area is located 6 km from the village of Granátula de Calatrava (Fig. 3a). Four subareas were considered: (i) Jabalón, (ii) NH-1, (iii) Fontecha and (iv) NH-2. In the Jabalón River, an elevated number of CO_2 -rich manifestations, bubbling into warm water ($<30^\circ\text{C}$) springs, occur, likely aligned along a fault system parallel (NW–SE) to the river bed (12 emission points in a profile of approximately 2 km). The location of the studied sites where CO_2 flux and radon measurements were carried out is shown in Fig. 3.

3.2. CO_2 flux measurements

Carbon dioxide soil fluxes were measured in 70 stations (Table 2, Fig. 3) using the accumulation chamber method (e.g., Cardellini et al., 2003; Chiodini et al., 1998), which is based on the continuous measurement of the CO_2 concentrations with time by using an inverted chamber placed on the ground. The accumulation chamber device consists of: (i) a metal cylindrical chamber with an inlet net area and inner volume of $3.14 \times 10^{-2} \text{ m}^2$ and $3.06 \times 10^{-3} \text{ m}^3$, respectively, (ii) an Infra-Red (IR) Spectrophotometer (Licor® Li-820, infra-red sensor detector, measuring range of 0–20,000 ppm, accuracy of 4% of readings), (iii) an analog–digital (AD) converter, and (iv) a palmtop computer (PC).

3.3. Radon measurements

The recording of the radon activity (70 points for ^{222}Rn and 31 for ^{220}Rn , respectively; Table 2, Fig. 3) was performed with two SARAD® RTM-2100 devices and one ionization chamber RADON V.O.S., model RM-2. Soil gases were collected with a stainless-steel hollow probe, which was hammered into the soil, down to a depth of 0.75–1.00 m in order to minimize the influence of atmospheric factors (e.g., King and Minissale, 1994). At La Sima, the probe was

inserted at the depth of 0.15–0.20 m due to the thin soil layer, which covered the bedrock. The radon monitor was fitted with a canister filled with drierite (97% $\text{CaSO}_4 + 3\% \text{CoCl}_2$) and a hydrophobic Teflon filter to minimize the humidity content within the instrument and preventing fine particles entering the ionization chamber (García-González et al., 2008). In the bubbling sites, radon measurements were carried out directly in the airflow, with a collector into which the bubbling gas was trapped.

The radon (^{222}Rn – ^{220}Rn) measurements were performed with a SARAD® RTM-2100 by analyzing the radon daughter isotopes ($^{218}\text{Po}/^{214}\text{Po}$ and ^{216}Po). The subsequent radioactive decay of these isotopes was recorded with a multichannel analyzer (alpha spectrometry). Soil gases were driven into the ionization chamber by an internal pump at the rate of 3 L min^{-1} . Measurements were carried out with the instrument in “thoron” mode and with integration time of 1 min. ^{222}Rn activity was assigned to the value of “radon” after 15 min and those of thoron after 5 min. After each series of measurements, the internal pump was set at high flow (3 L min^{-1}) for 20–30 min to clean the ionization chamber before starting a new measurement. The detection limit of the instrument was 1 kBq m^{-3} , and the statistical error at 1σ was defined as $100\%/\sqrt{N}$, where N is the number of registered counts of the relevant nuclides ($^{218}\text{Po}/^{214}\text{Po}$ and ^{216}Po) within the time interval. For an Equivalent Radon Concentration of 1 kBq m^{-3} or higher the statistical error was below 10%.

The RM-2 system was designed for the determination of soil gas radon (^{222}Rn) concentrations. The detection principle consists in an ionization chamber where a potential difference between a positively charged metal outer shell and an electrode located along the longitudinal axis (0 V) was applied. When radon emits alpha particles, ions were detected by the electrode. The ion current was then measured and converted to Rn concentration, expressed as Bq m^{-3} . The soil gas was collected with a 150 mL syringe, connected to the top of a stainless-steel hollow probe and transferred into a pre-evacuated ionization chamber (250 mL). Pressure inside the chamber was equalized to the ambient atmospheric pressure by opening the valve. Measurements were carried out after 15 min. The delay of 15 min ensured that the activity of ^{220}Rn was practically negligible due to its short half-life. The detection limit was 5 kBq m^{-3} . The uncertainty of radon concentration (1σ) was $0.33(C_{\text{rn}})^{0.5}$, where C_{rn} is the radon concentration ($C_{\text{rn}} \pm \sigma$). The RM-2 error of the radon concentration was below 15%.

Radon concentrations (^{222}Rn [Bq m^{-3}]) obtained with the two instrumentation (SARAD® RTM-2100 and RM-2) did not significantly differ (relative standard deviation – RSD – around 10%). Thus, the ^{222}Rn concentrations were analyzed independently of the instrument, and will not be discussed further.

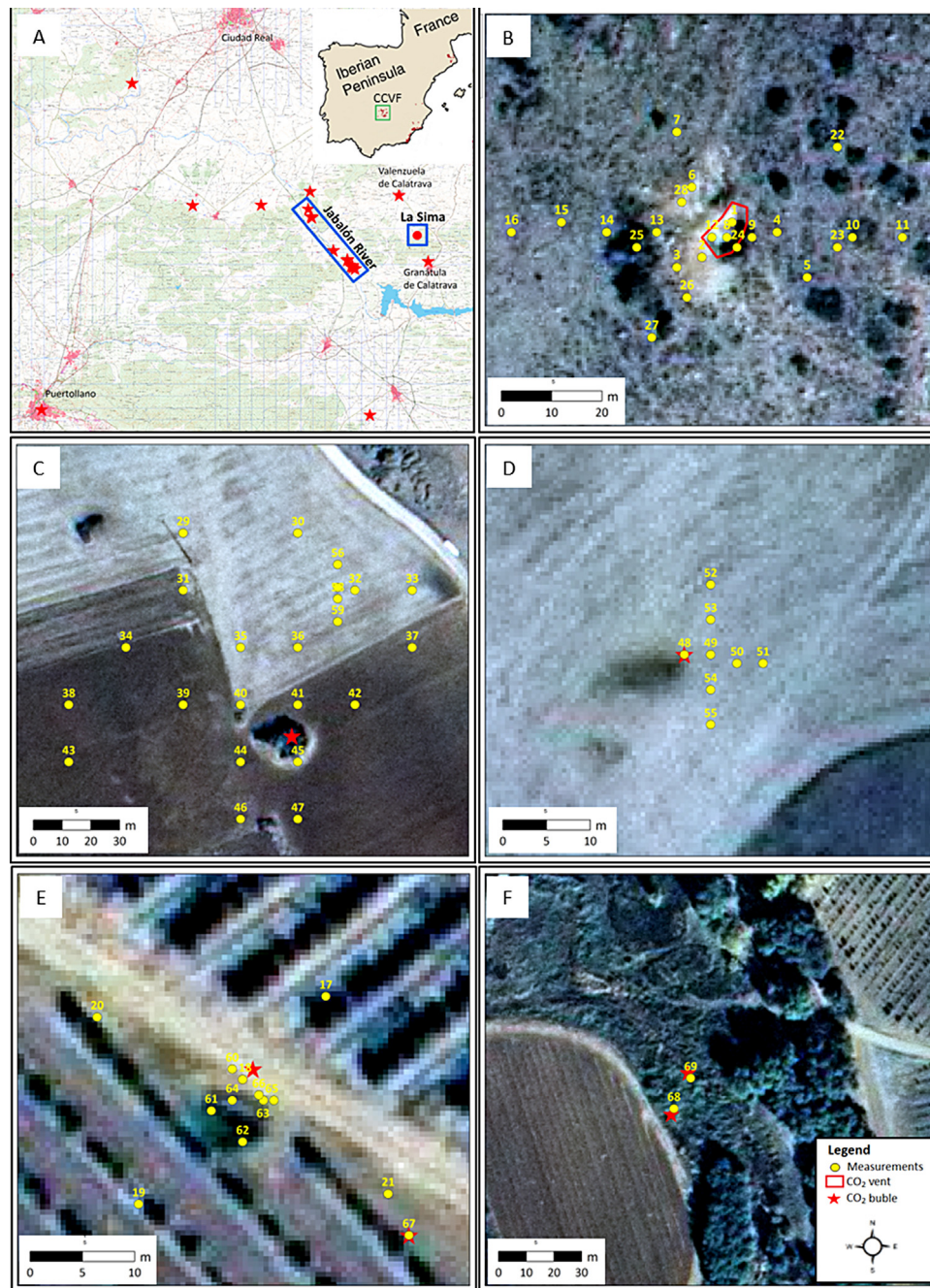


Fig. 3. Sampling zones: (a) CCVF area, (b) La Sima, (c) Jabalón, (d) NH-1, (e) Fontecha and (f) NH-2.

3.4. Soil sampling

Eight soil samples (Table 3; Fig. 3) were collected to measure the concentration of the radon parent radionuclides (U–Ra) and to assess whether radon was originated by the soil cover or was transferred from deep sources by advective circulation. Sampling was carried out with an Edelman auger at the same depth where the soil-gases were measured: two at La Sima gas vent (inside and outside the degassing site) and six at the Jabalón River area (2 close to the CO₂ seepage, i.e., where CO₂ was bubbling in water, and 4 at a distance of 10–30 m). Samples were analyzed by gamma-ray spectrometry (Quindós et al., 2006) at the Department of Medical Physics, Faculty of Medicine (University of Cantabria, Spain). The ²²⁶Ra concentrations in soils provided the theoretical ²²²Rn concentrations, which were estimated according to Eq. (1).

Since ε , ρ and n were not measured, the distribution of the theoretical concentration of ²²²Rn was estimated by Monte Carlo simulation, assuming that ε , ρ and n were normally distributed with the typical values of gravel, sand and clay (Table 1; Yu et al., 1993). The theoretical concentration was interpreted as a geochemical threshold. Hence, in the case that the soil was the only source

Table 1
Typical ε , ρ and n values in soil.

Parameter	Minimum	Mean	Maximum
ε	0.18	0.29	0.40
ρ (kg m ⁻³)	1200	1350	1500
n	0.01	0.30	0.50

Source: Yu et al. (1993).

of ^{222}Rn , which was related to the presence of ^{226}Ra , the measured activity was expected to be similar to the calculated content. If ^{222}Rn activity was higher than this threshold radon was interpreted to be deep-sourced.

4. Results

To avoid possible interpretation errors originated by the influence of water to the activity of radon in the soil-gas, the geochemical analyses were divided into two types of emissions: (i) La Sima (dry gas vent) and (ii) Jabalón River (CO_2 -rich gases bubbling in water).

4.1. La Sima

The soil CO_2 flux ranged from 0.20 to $5379 \text{ g m}^{-2} \text{ d}^{-1}$, although inside the morphological depression of La Sima the CO_2 flux was not measured as the IR detector saturated in a few seconds (i.e., $>20,000 \text{ ppm s}^{-1}$ of CO_2). The ^{222}Rn activity in soil also showed a relatively wide range, between 0.64 and 138 kBq m^{-3} . The ^{220}Rn contents were more constant and ranged between 7.6 and 51.7 kBq m^{-3} (Table 2).

Five out of the 23 CO_2 flux measurements at La Sima (Table 2, Fig. 3b) were considered anomalous [higher than $Q_3 + 1.5 \times (Q_3 - Q_1)$, being Q_1 and Q_3 the first and the third quartile, respectively], i.e., #13 ($45 \text{ g m}^{-2} \text{ d}^{-1}$), #12 ($196 \text{ g m}^{-2} \text{ d}^{-1}$), #8 ($566 \text{ g m}^{-2} \text{ d}^{-1}$), #24 ($3322 \text{ g m}^{-2} \text{ d}^{-1}$) and #1 ($5379 \text{ g m}^{-2} \text{ d}^{-1}$). These anomalous points were located inside the depression of La Sima (#1, 8 and 24) or very close (#12) to it, suggesting that the CO_2 seepage was well restricted to very small area (red zone in Fig. 3b).

Radium activity (^{226}Ra) was similar inside and outside the emission site, with an average value clustering around 40 Bq kg^{-3} (Table 3). From Eq. (1), the theoretical concentration of radon (^{222}Rn), inside and outside the CO_2 emission, was estimated to be 55 kBq m^{-3} (Table 4), with 95% of the data below 82 kBq m^{-3} (Table 4).

4.2. Jabalón River

All studied subareas along the Jabalón River were related to spring water discharges ($T < 30^\circ\text{C}$) where a CO_2 -rich gas phase was gently-to-vigorously bubbling. The CO_2 fluxes were from <0.2 ($<\text{D.L.}$) to $1 \times 10^6 \text{ g m}^{-2} \text{ d}^{-1}$. In some cases the CO_2 flux was not measured as the IR detector instantly saturated. Occasionally, high CO_2 fluxes (up to $1 \text{ t m}^{-2} \text{ d}^{-1}$ or even higher) were measured, although at a short distance, even at the scale of few decimeters, a dramatic decrease was recorded, and the CO_2 fluxes, typical of biologic respiration (0.02 – $18 \text{ g m}^{-2} \text{ d}^{-1}$; Elío et al., 2013 and reference therein; Fig. 4), were determined. The lowest activity of ^{222}Rn was 2.3 kBq m^{-3} whilst the highest one was 428 kBq m^{-3} . The concentrations of ^{220}Rn ranged from 9.0 to 44.5 kBq m^{-3} (Table 2).

The results by gamma-ray spectrometry (Table 3) showed that there was a difference in the ^{226}Ra concentration between the sites close to the leaking points (#41 and #45) and away from them (#30, #42, #A and #B). While near the main CO_2 -rich sources the ^{226}Ra concentration was approximately 70 Bq kg^{-1} , in the distal zones its content abruptly decreased down to 30 Bq kg^{-1} . The difference in radium concentration produced two theoretical ^{222}Rn activities for the soil gas due to the presence of ^{226}Ra in the Jabalón River area. The ^{222}Rn activity for those soil gas located far from the water springs was around 40 kBq m^{-3} , with 95% of the data below 60 kBq m^{-3} . This value increased up to 95 kBq m^{-3} , with 95% of the data below 140 kBq m^{-3} , near the water springs (Table 4).

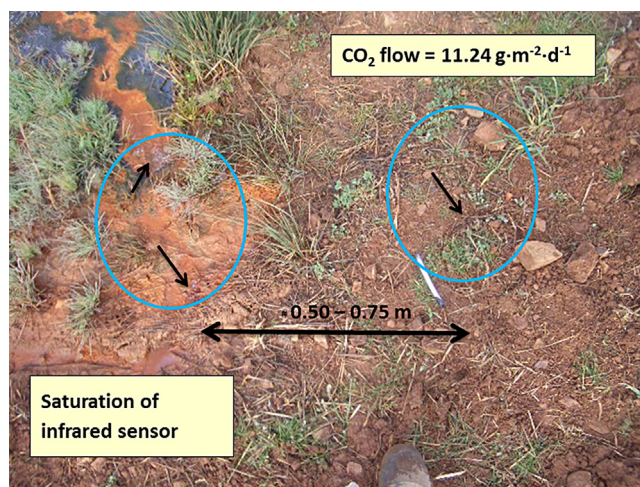


Fig. 4. Example of very high CO_2 flow through very small spots. To the left, the IR detector saturated in a few seconds; a few centimeters to the right, the CO_2 soil flux showed values, which can be related to a background emission, i.e., biological activity.

5. Discussion

5.1. La Sima

5.1.1. Theoretical ^{222}Rn concentration in soil-gas

At La Sima, most ^{222}Rn measurements were between 0.6 and 37.2 kBq m^{-3} , i.e., slightly lower than the theoretical estimation (approximately 55 kBq m^{-3} ; Table 4). As previously mentioned, the lack of a developed soil cover partly prevented the radon measurement, which was made at the depth of 0.15 – 0.20 cm , where the influence of the atmospheric parameters can significantly affect the radon concentrations. However, despite the discrepancy between the theoretical and measured values and the uncertainty of the field measurements (below 10 – 15%) and the theoretical estimations, it is reasonable to assume that the threshold in this zone was of 45 – 60 kBq m^{-3} . Such high concentrations cannot be explained with the presence of ^{226}Ra in the soil and consequently, a deep Rn source is required. This value was exceeded in four points (#12: 63 kBq m^{-3} ; #1: 117 kBq m^{-3} ; #8: 118 kBq m^{-3} and #24: 138 kBq m^{-3}).

5.1.2. Correlation between CO_2 flux and radon (^{222}Rn – ^{220}Rn) activity in soil-gas

Setting aside #13, which had a CO_2 flux value of $45 \text{ g m}^{-2} \text{ d}^{-1}$, four anomalous data were measured at La Sima, #12 ($196 \text{ g m}^{-2} \text{ d}^{-1}$), #8 ($566 \text{ g m}^{-2} \text{ d}^{-1}$), #24 ($3322 \text{ g m}^{-2} \text{ d}^{-1}$) and #1 ($5379 \text{ g m}^{-2} \text{ d}^{-1}$), likely associated with the occurrence of a deep-seated flow that affects the soil degassing in this area. When comparing the CO_2 flux and the ^{222}Rn activity data, we observed that the higher the CO_2 flux the higher the Rn activities (#1, #24, #8 and #12; Fig. 5a). These sites are those whose ^{222}Rn concentrations cannot be explained without invoking a deep radon source. Conversely, where low CO_2 fluxes were measured the ^{222}Rn values can be associated with the presence of ^{226}Ra in the soil.

The ^{220}Rn concentrations are inversely correlated with the CO_2 flux values (Fig. 5b). The relatively high $^{222}\text{Rn}/^{220}\text{Rn}$ ratios (up to 20 ; Fig. 5c) are likely associated with a deep origin of radon. This is also supported by the $\delta^{13}\text{C}$ – CO_2 and $^3\text{He}/^4\text{He}$ isotopic values, which suggest a deep (mantle) root for the CCVF gas discharges (Pérez et al., 1996; Vaselli et al., 2013).

The relationship between the highest CO_2 fluxes and ^{222}Rn concentrations is well illustrated when plotting the W–E oriented

Table 2Soil CO₂ gas flux (in g m⁻² d⁻¹) and ²²²Rn and ²²⁰Rn (in kBq m⁻³) measurements. Coordinates are in UTM-WGS84 projection, zone 30N.

Site	Data	Sample	Est	North	CO ₂ flux (g m ⁻² d ⁻¹)	²²² Rn (kBq m ⁻³)	²²⁰ Rn (kBq m ⁻³)	Observation
La Sima	June 10	1	434,419	4,297,245	5379	116.8	7.6	Soil-gas
La Sima	June 10	2	434,413	4,297,238	0.4	0.64		Soil-gas
La Sima	June 10	3	434,408	4,297,236	0.3	1.2		Soil-gas
La Sima	June 10	4	434,428	4,297,243	4.3	1.7		Soil-gas
La Sima	June 10	5	434,434	4,297,234	2.1	6.6		Soil-gas
La Sima	June 10	6	434,411	4,297,252	1.3	9.7		Soil-gas
La Sima	June 10	7	434,408	4,297,263	1.5	5.7		Soil-gas
La Sima	August 10	8	434,418	4,297,242	567	118.4	13.3	Soil-gas
La Sima	August 10	9	434,423	4,297,242	5.4	3.1	31.1	Soil-gas
La Sima	August 10	10	434,443	4,297,242	0.2	11.1	34.0	Soil-gas
La Sima	August 10	11	434,453	4,297,242	0.6	6.6	26.7	Soil-gas
La Sima	August 10	12	434,415	4,297,242	196	63.2	10.4	Soil-gas
La Sima	August 10	13	434,404	4,297,243	45	10.5		Soil-gas
La Sima	August 10	14	434,394	4,297,243	7.1	10.2	23.0	Soil-gas
La Sima	August 10	15	434,385	4,297,245	0.2	13.0	32.7	Soil-gas
La Sima	August 10	16	434,375	4,297,243	0.5	11.5	51.7	Soil-gas
Fontecha	May 11	17	428,709	4,295,194	7.3	58.0		Soil-gas
Fontecha	May 11	18	428,701	4,295,186	192	428.0		Soil-gas
Fontecha	May 11	19	428,691	4,295,174	12.3	3.0		Soil-gas
Fontecha	May 11	20	428,687	4,295,192	17.9	39.7		Soil-gas
Fontecha	May 11	21	428,715	4,295,175	15.8	2.3		Soil-gas
La Sima	May 11	22	434,440	4,297,260	7.6	9.8		Soil-gas
La Sima	May 11	23	434,440	4,297,240	4.2	3.0		Soil-gas
La Sima	May 11	24	434,420	4,297,240	3322	138.0		Soil-gas
La Sima	May 11	25	434,400	4,297,240	5.5	37.2		Soil-gas
La Sima	May 11	26	434,410	4,297,230	5.7	16.7		Soil-gas
La Sima	May 11	27	434,403	4,297,222	18.0	34.0		Soil-gas
La Sima	May 11	28	434,409	4,297,249	3.1	11.5		Soil-gas
Jabalón	September 11	29	429,130	4,294,625	1.4	32.4		Soil-gas
Jabalón	September 11	30	429,170	4,294,625	44	83.1	27.0	Soil-gas
Jabalón	September 11	31	429,130	4,294,605	5.3	29.1	9.0	Soil-gas
Jabalón	September 11	32	429,190	4,294,605	21.9	28.2		Soil-gas
Jabalón	September 11	33	429,210	4,294,605	12.3	24.5	28.5	Soil-gas
Jabalón	September 11	34	429,110	4,294,585	<0.2	25.6	15.5	Soil-gas
Jabalón	September 11	35	429,150	4,294,585	5.1	12.2	17.8	Soil-gas
Jabalón	September 11	36	429,170	4,294,585	11.6	47.0	10.5	Soil-gas
Jabalón	September 11	37	429,210	4,294,585	9.6	49.7		Soil-gas
Jabalón	September 11	38	429,090	4,294,565	<0.2	18.6	11.2	Soil-gas
Jabalón	September 11	39	429,130	4,294,565	2.9	22.7	12.3	Soil-gas
Jabalón	September 11	40	429,150	4,294,565	25.7	34.2	30.8	Soil-gas
Jabalón	September 11	41	429,170	4,294,565	45	182.5	35.2	Soil-gas
Jabalón	September 11	42	429,190	4,294,565	102	91.1	31.6	Soil-gas
Jabalón	September 11	43	429,090	4,294,545	<0.2	24.2	19.4	Soil-gas
Jabalón	September 11	44	429,150	4,294,545	5.7	13.2	24.0	Soil-gas
Jabalón	September 11	45	429,170	4,294,545	141	183.5	18.4	Soil-gas
Jabalón	September 11	46	429,150	4,294,525	5.2	7.8		Soil-gas
Jabalón	September 11	47	429,170	4,294,525	0.5	17.3	13.9	Soil-gas
NH-1	February 12	48.5	429,137.5	4,294,759	913,887	118.0		Bubbling pool
NH-1	February 12	48	429,137	4,294,759	523,140	130.0		Bubbling pool
NH-1	February 12	49	429,140	4,294,759	4.6	171.0	11.5	Soil-gas
NH-1	February 12	50	429,143	4,294,758	7.1	56.1		Soil-gas
NH-1	February 12	51	429,146	4,294,758	8.9	37.8		Soil-gas
NH-1	February 12	52	429,140	4,294,767	0.3	39.7	44.5	Soil-gas
NH-1	February 12	53	429,140	4,294,763	1.6	60.6	23.5	Soil-gas
NH-1	February 12	54	429,140	4,294,755	0.9	55.6	39.5	Soil-gas
NH-1	February 12	55	429,140	4,294,751	7.4	42.2	38.2	Soil-gas
Fontecha	February 12	56	429,184	4,294,614	3.2	23.2		Soil-gas
Fontecha	February 12	57	429,184	4,294,606	9.0	8.9		Soil-gas
Fontecha	February 12	58	429,184	4,294,602	1.4	59.0		Soil-gas
Fontecha	February 12	59	429,184	4,294,594	241	15.6	10.8	Soil-gas
Fontecha	February 12	60	428,700	4,295,187	1.2	75.1		Soil-gas
Fontecha	February 12	61	428,698	4,295,183	8.6	82.6		Soil-gas
Fontecha	February 12	62	428,701	4,295,180	6.6	421.9	27.9	Soil-gas
Fontecha	February 12	63	428,704	4,295,184	8.1	154.0		Soil-gas
Fontecha	February 12	64	428,700	4,295,184	7.1	218.0		Soil-gas
Fontecha	February 12	65	428,703	4,295,184	918,290	129.0		Bubbling pool
Fontecha	February 12	66	428,703	4,295,185	548,485	92.4		Bubbling pool
Fontecha	February 12	67	428,717	4,295,171	35,821	54.1		Bubbling pool
NH-2	February 12	68	427,578	4,295,993	684	13.5		Bubbling pool
NH-2	February 12	69	427,584	4,296,004	180	15.5		Bubbling pool

Table 3
Results of gamma-ray spectrometry in soil samples.

Site	Sample	^{238}U (^{234}Th)	^{226}Ra (^{214}Bi)	^{232}Th (^{228}Ac)	^{40}K	^{137}Cs
La Sima	Outside	79.0 ± 10.8	40.2 ± 1.5	70.4 ± 4.5	775.5 ± 32.2	<D.L. (1.2)
	Inside	86.3 ± 11.5	40.9 ± 1.6	117.3 ± 7.2	694.8 ± 29.9	31.6 ± 1.0
Jabalón River	30	26.2 ± 3.9	34.0 ± 1.4	64.5 ± 4.4	984.9 ± 40.2	<D.L. (1.4)
	A	<D.L. (25.4)	23.0 ± 1.2	79.2 ± 5.0	776.3 ± 33.0	<D.L. (1.7)
	42	39.5 ± 8.5	26.5 ± 1.3	71.1 ± 4.9	871.8 ± 35.6	<D.L. (1.8)
	41	137.8 ± 14.9	76.0 ± 2.2	72.9 ± 4.9	962.3 ± 39.7	<D.L. (1.8)
	45	<D.L. (27.6)	69.5 ± 2.1	71.0 ± 4.7	935.4 ± 39.2	<D.L. (1.8)
	B	<D.L. (24.9)	35.4 ± 1.4	57.6 ± 3.9	742.6 ± 30.9	<D.L. (1.6)

Concentrations are in Bq kg^{-1} . Points A and B not shown in Fig. 3.

Table 4
Theoretical concentrations of ^{222}Rn (in Bq m^{-3}) in soil gas as calculated by ^{226}Ra decay in the soil.

Site	^{226}Ra (Bq kg^{-1})	^{222}Rn (kBq m^{-3})						
		Min.	Q_1	Median	Mean	Q_3	95th percentile	Max.
La Sima	40	23	44	51	54	61	82	452
Jabalón River (away bubbling)	30	17	33	38	41	46	61	339
Jabalón River (near bubbling)	70	40	77	90	95	107	143	791

profile (Fig. 6) as a function of the distance from La Sima gas vent. Another relevant result was that at #8 (distance 0 m) the highest concentration of ^{222}Rn was recorded while that of ^{220}Rn was among the lowest measured values. This might be explained with the dilution of a ^{220}Rn -free deep gas as it rises to the surface. Furthermore, the amount of ^{220}Rn generated at the surface was promptly released

once produced because of the elevated CO_2 -rich gas flux and, consequently, the recorded data were smaller than those really produced. The highest $^{222}\text{Rn}/^{220}\text{Rn}$ ratios were at #8 (La Sima) and #12, suggesting a predominance of the highest half-life isotope (^{222}Rn). These results demonstrate that CO_2 acts as a carrier gas for radon in a regime of advective transport.

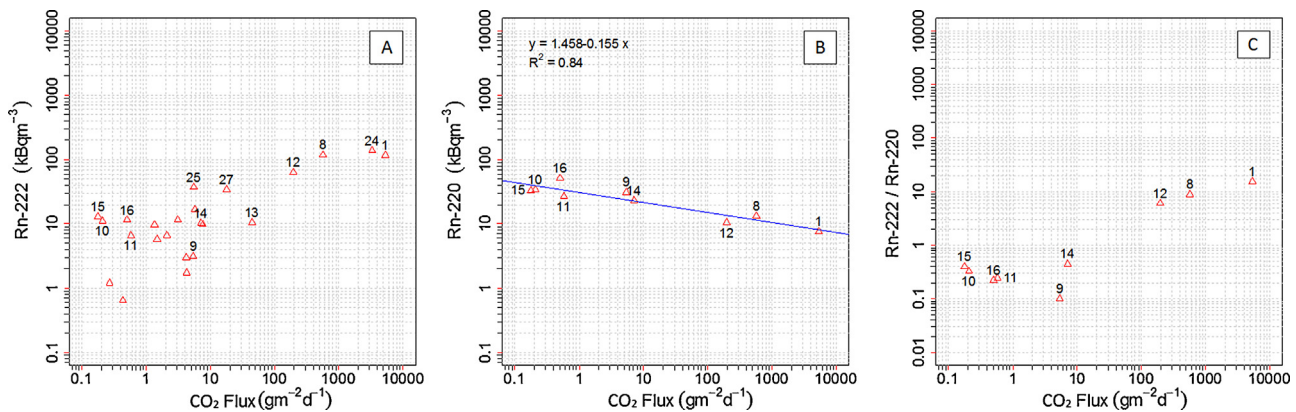


Fig. 5. Relationship between CO_2 flux and $^{222}\text{Rn}/^{220}\text{Rn}$ in the La Sima zone (Table 2, Fig. 3).

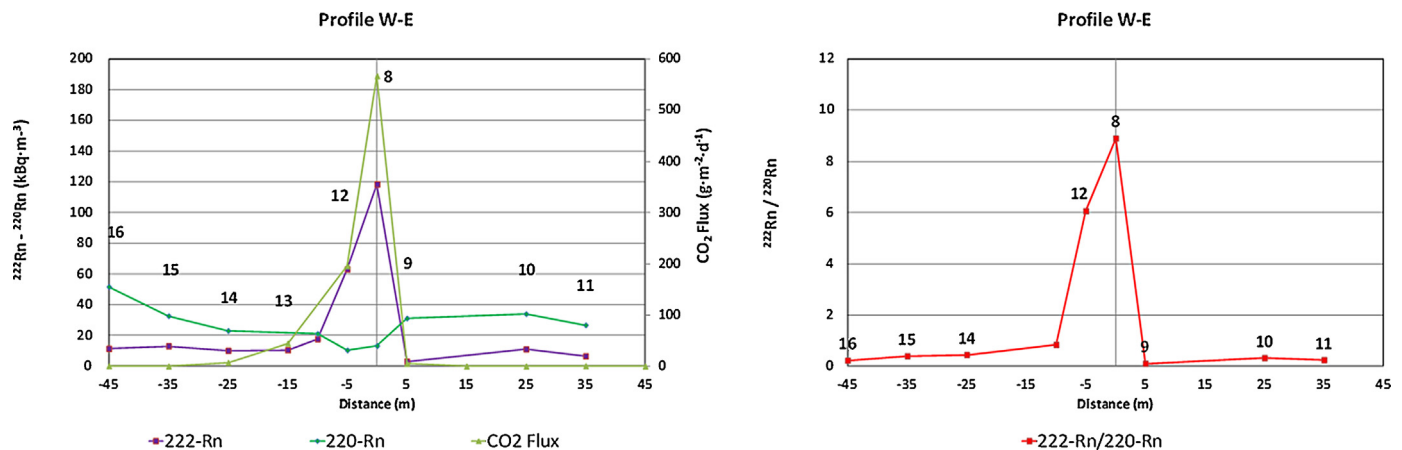


Fig. 6. Spatial correlation between $^{222}\text{Rn}/^{220}\text{Rn}$ and CO_2 flux in the La Sima zone (Table 2, Fig. 3). Horizontal axis is the distance (m) from the sample point to the center of the CO_2 leak.

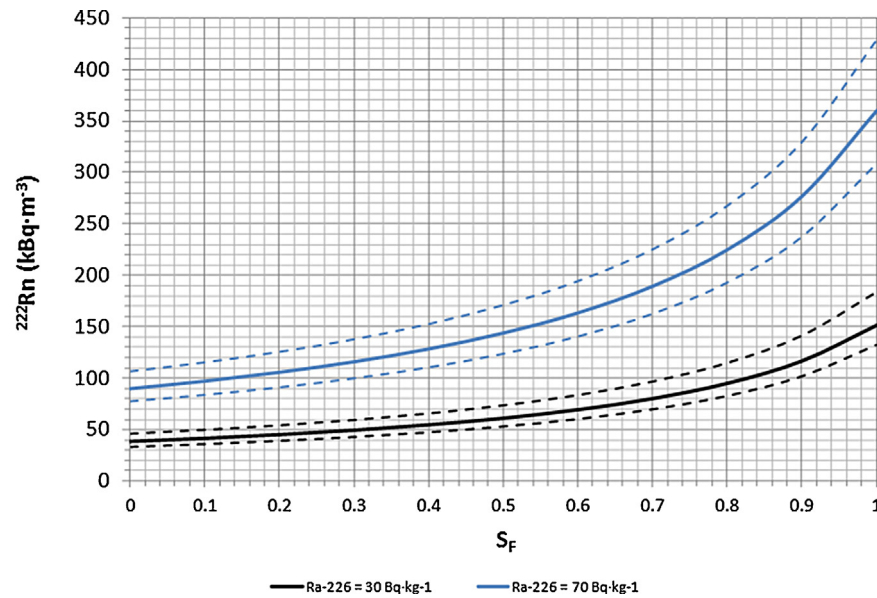


Fig. 7. Equilibrium ^{222}Rn activity of the soil-gas in the area of Jabalón River versus ^{226}Ra activity. Black and blue lines represent a radium activity of 30 Bq kg^{-1} and 70 Bq kg^{-1} , respectively. Continuous lines are the median of theoretical radon concentration and dotted lines are referred to the first (Q_1) and the third (Q_3) quantile (Table 4). (For interpretation of the references to color in this figure legend, the reader is referred to the web version of this article.)

5.2. Jabalón River

5.2.1. Theoretical ^{222}Rn activity in soil-gas

The increase of ^{226}Ra activity between the sites located away from the thermal waters (30 Bq kg^{-1}) and those close to them (70 Bq kg^{-1}) could be produced by a process of transport of dissolved U and Ra and their precipitation at the spring. Thus, two theoretical ^{222}Rn concentrations were carried out, although in this case the influence of soil water saturation (S_F ; Eq. (2)) are to be taken into account for the interpretation of the gas ^{222}Rn origin. The radon activity equilibrium of the soil gas is plotted in Fig. 7. In order to evaluate the influence on the radon measurements produced by the water contained in the soil, a distinction between the Ra concentrations was made. In those points located far from the water springs, the soil is expected to be relatively dry or slightly moist ($S_F \approx 0.1\text{--}0.5$). This would imply that the increase of ^{222}Rn from the water contained in the soil should not exceed more than 50% of the theoretical concentration for dry soil ($\approx 70\text{ kBq m}^{-3}$; black lines in Fig. 7). Thus, the concentration of Ra in the soil does not account for the ^{222}Rn concentrations in soil gases when they are much higher than $40\text{--}70\text{ kBq m}^{-3}$. Close to the water springs, where soils are expected to be relatively moist ($S_F \approx 0.5\text{--}0.8$), the radon concentration can increase of 50–150% with respect to dry conditions; therefore the theoretical activity of ^{222}Rn could be around 120 kBq m^{-3} (black lines in Fig. 7). If the transport of radium is driven by ground water, the ^{222}Rn content is expected to increase up to 270 kBq m^{-3} (blue lines in Fig. 7).

In these areas, the points located at a distance from the water springs were commonly characterized by radon activity values less than 70 kBq m^{-3} , which are in agreement with those calculated with the presence of ^{226}Ra in the relatively dry soil, e.g., #17, #20, #32 and #35 (Table 2; Fig. 3). However, this threshold was exceeded at two points: #30 (83 kBq m^{-3}) and #42 (91 kBq m^{-3}), which are unlikely values for dry/moderately moist soils. This would imply a more efficient advective transport and/or a deep gas source.

In proximity to the water springs (#18, #41, #45, #49–55, #60–64; Table 2 and Fig. 3), the ^{222}Rn activity was between 38 (#51) and 428 kBq m^{-3} (#18). As previously described, the radon activity can increase to 120 kBq m^{-3} due to presence of water in the soil. Actually, some high ^{222}Rn values (from 56 to 83 kBq m^{-3} ,

e.g., #50, #53, #60 and #61) could be related to the increase in water saturation. Nevertheless, very high values were also measured at #63 (154 kBq m^{-3}), #49 (171 kBq m^{-3}), #41 (182 kBq m^{-3}), #45 (183 kBq m^{-3}), #64 (218 kBq m^{-3}), #62 (421 kBq m^{-3}) and #18 (428 kBq m^{-3}). Radon activity at #63, #49, #41, #45 and #64 can be attributed to soil moisture when the radium content is up to 70 Bq kg^{-1} (blue line in Fig. 7). However, radon activities higher than 270 kBq m^{-3} are unlikely when increases in radium content and soil moisture are considered. Consequently, also in this case, the contribution by a deep source can be invoked (e.g., #62 and #18). We may speculate that in addition to the increase of radon concentration by water saturation in the soil, an excess of ^{222}Rn is likely occurring and favored by the presence of parent radionuclides (U and Ra) dissolved in the ground water system.

5.2.2. Correlation between CO_2 flux and radon (^{222}Rn – ^{220}Rn) activity in soil-gas

At Jabalón River the highest activities of ^{222}Rn and CO_2 fluxes are not apparently closely correlated (Fig. 8a). Nevertheless, ^{222}Rn contents higher than those estimated by the presence of ^{226}Ra in the soil were detected in sites close to the thermal springs (e.g., #18 and #62) and away from them (e.g., #30 and #42), suggesting the presence of a deep ^{222}Rn source. However, ^{222}Rn activity near the spring waters (blue-colored numbers in Fig. 8a) was always higher than those measured in the distal points (black-colored numbers in Fig. 8a), although CO_2 fluxes were relatively low (e.g., #62 and #64 versus #30, #42 or #59). An inverse correlation between ^{220}Rn and CO_2 was not observed (Fig. 8b). On the other hand, ^{220}Rn had a small increase (Fig. 9), which could be interpreted in terms of shallow origin of radon, at least more superficial than that of La Sima. This could likely be accounted for the transport and precipitation of U and Ra. In relation to the $^{222}\text{Rn}/^{220}\text{Rn}$ ratio (Fig. 8c) there was not a clear increase with the CO_2 flux in contrast to what observed at La Sima. Despite the relatively high isotopic ratio (e.g., #49, #62, #45), no correlation with the CO_2 flux was highlighted since in some cases the $^{222}\text{Rn}/^{220}\text{Rn}$ ratio decreased (e.g., #59 vs #36 or #49). Similar features can be produced by either deep or shallow origin for radon and by the soil water saturation.

These results suggest that the increase of radon activity in the Jabalón River with respect to the background is likely related to two

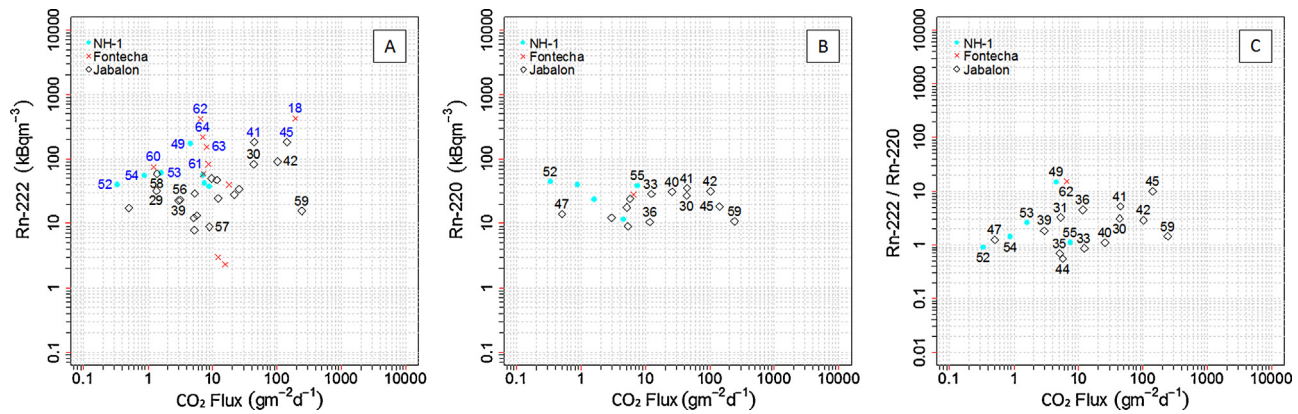


Fig. 8. Relationship between CO_2 flux and $^{222}\text{Rn}/^{220}\text{Rn}$ ratios in the Jabalón River (blue texts in A indicate the points near water spring, Table 2, Fig. 3). (For interpretation of the references to color in this figure legend, the reader is referred to the web version of this article.)

contributions: (i) a deep-seated source carried by CO_2 , supported by the higher concentrations of ^{222}Rn with respect to those theoretically estimated by ^{226}Ra in soil, and (ii) a source related to the decay of parent radionuclides (U–Ra), dissolved and transported by groundwater system as supported by the highest radium activities when approaching the spring water discharges.

The profiles of the CO_2 flux as a function of the distance with respect to the CO_2 -rich gas emission sites and those of the Rn isotopic concentration and $^{222}\text{Rn}/^{220}\text{Rn}$ ratios for the Jabalón River are plotted in Figs. 9 and 10. In Fig. 9a and b (profile N–S for Jabalón, Fig. 3c, Table 2), the highest value of CO_2 flux (#45, $141 \text{ g m}^{-2} \text{ d}^{-1}$) is

coupled with that of ^{222}Rn (184 kBq m^{-3}), although at #41 the CO_2 flux sharply decreases down to $45 \text{ g m}^{-2} \text{ d}^{-1}$ while the Rn activity was found to be constant (182 kBq m^{-3}). Moving to the north of the CO_2 -bearing spring (#36) both activity of ^{222}Rn and CO_2 flux (47 kBq m^{-3} and $12 \text{ g m}^{-2} \text{ d}^{-1}$, respectively) decrease. Then, the ^{222}Rn activity achieves a secondary peak (#30: 83 kBq m^{-3}), which is not related to any increase of ^{226}Ra in the soil (Table 3), while the CO_2 flux increases ($44 \text{ g m}^{-2} \text{ d}^{-1}$). In contrast, in the E–W profile (Fig. 9c and d) the highest recorded CO_2 flux (#42; $102 \text{ g m}^{-2} \text{ d}^{-1}$) does not match with that of the ^{222}Rn activity (#41; 182 kBq m^{-3}). The activity of ^{220}Rn in both profiles shows an increase associated

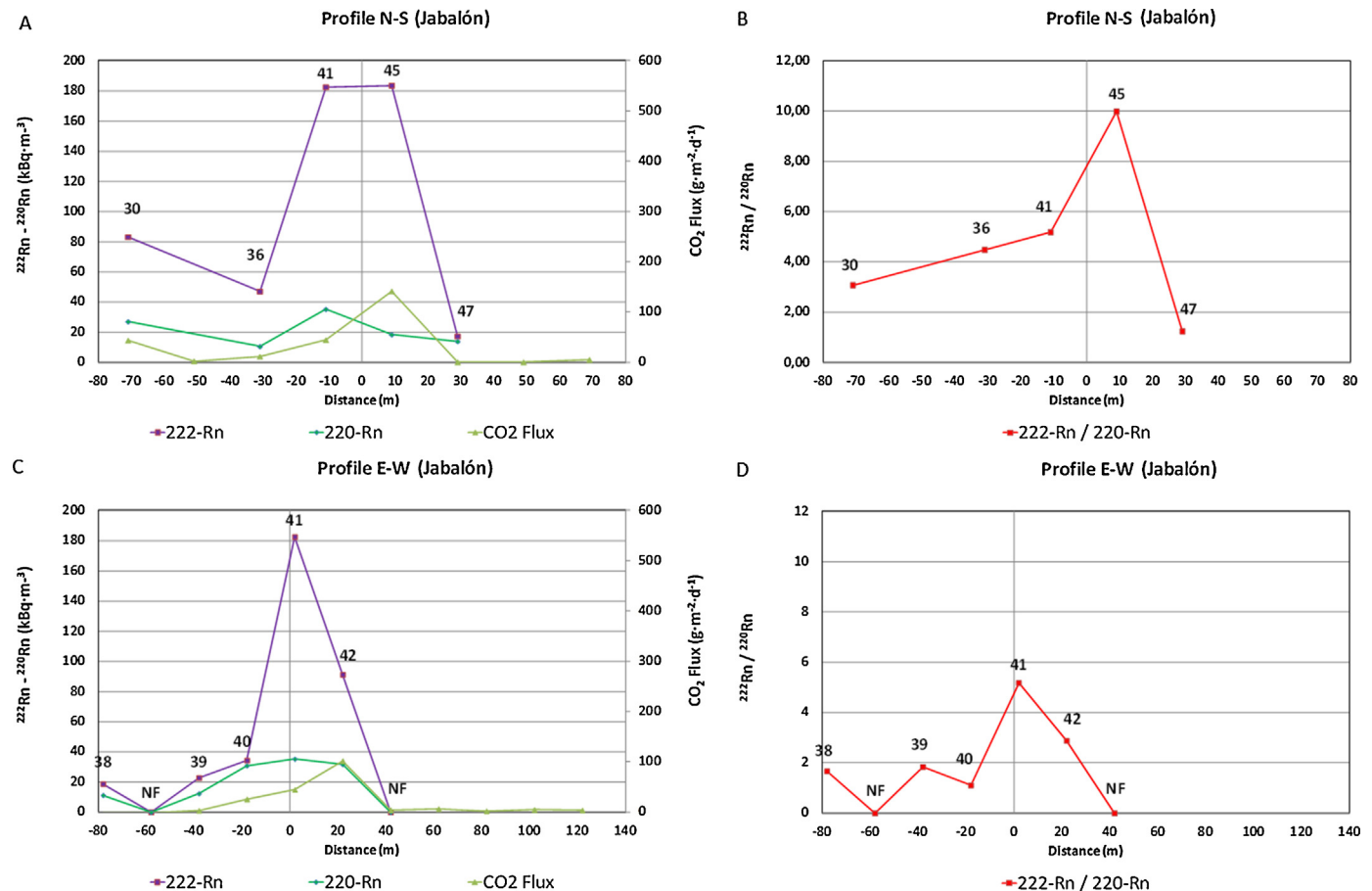


Fig. 9. Spatial correlation between $^{222}\text{Rn}/^{220}\text{Rn}$ and CO_2 flux along the Jabalón River (Table 2, Fig. 3; NF: no flow, soil-gas could not be sampled due to the extremely low permeability). Horizontal axis is the distance (m) from the sample point to the center of the CO_2 leak.

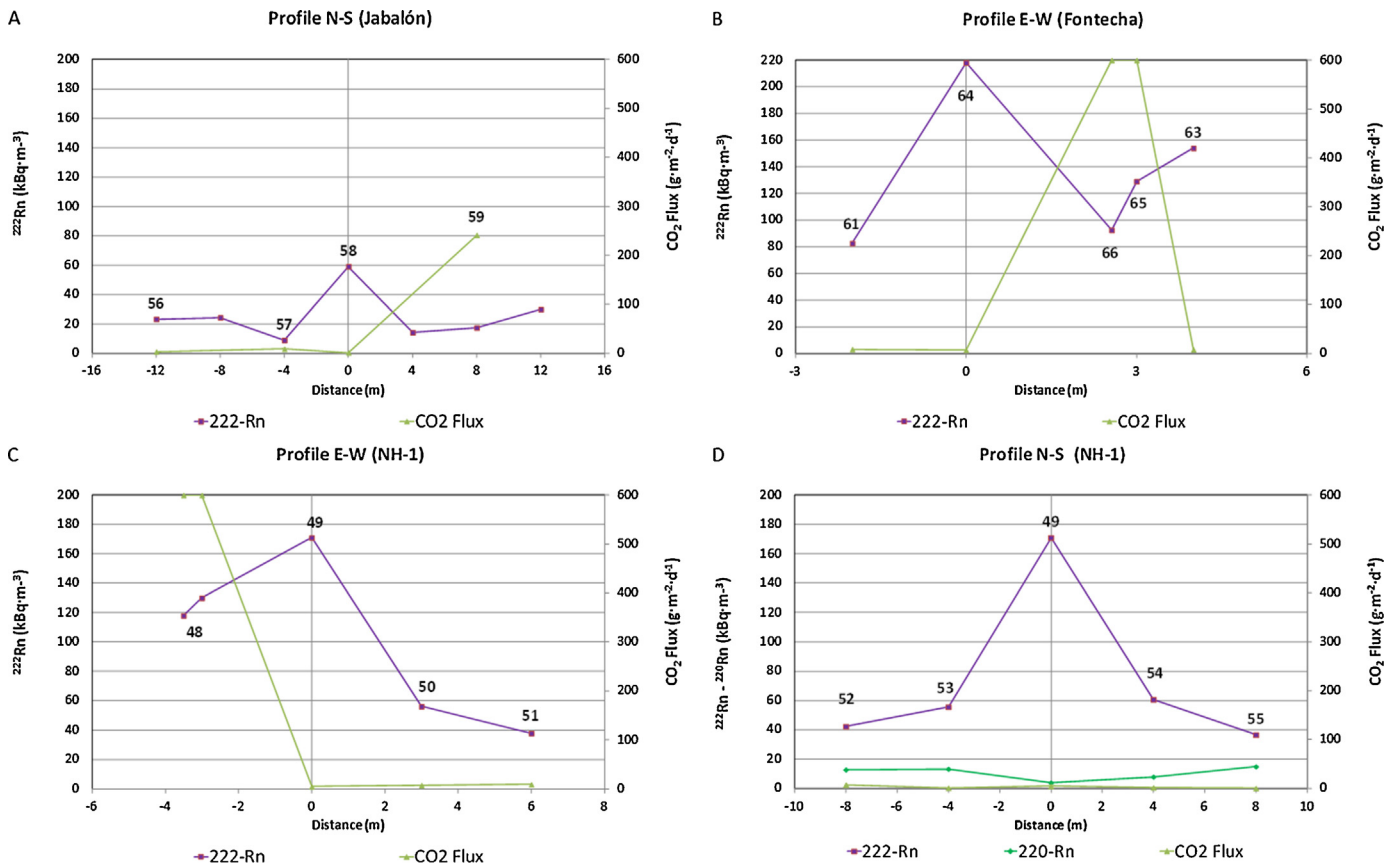


Fig. 10. Spatial correlation between $^{222}\text{Rn}/^{220}\text{Rn}$ and CO_2 flux along the Jabalón River (Table 2, Fig. 3). Horizontal axis is the distance (m) from the sample point to the center of the CO_2 leak.

with the CO_2 flux, although the highest ^{220}Rn concentration (#41) does not completely match with respect to the site where the highest CO_2 flux (#45 in profile N-S and #42 in profile E-W in Fig. 9a and b) is found.

In Fig. 10, the lack of correlation between the highest values of ^{222}Rn concentration and CO_2 flux for the same spot is more evident. Nevertheless, despite the fact that a linear correlation between CO_2 and ^{222}Rn is not detected, there is a direct influence in radon (^{222}Rn) activity associated with the CO_2 leakage. This is supported by the presence of ^{222}Rn concentrations near the seepage zones much higher than those calculated by considering the Ra concentrations in the soil or the increase related to soil water saturation.

In the springs with bubbling CO_2 (#48, #65 to #68; Table 2, Fig. 11) the ^{222}Rn activity is lower with respect to that measured in the surrounding sites. This discrepancy can likely be due to the different sampling methods since in these spots radon measurements were carried out directly in the airflow, with a collector on the bubbling gas phase due to the presence of water. Consequently, these measurements can be related to the amount of ^{222}Rn carried by CO_2 and not to the content of U and Ra in the thermal waters or the presence of soil water saturation (S_F). Nevertheless, in the soil-gas near the degassing sites all effects could be detected and therefore the radon concentration in the gas is higher. The positive linear correlation between the CO_2 flux and concentration of ^{222}Rn in the gas vent is supporting this hypothesis (Fig. 11).

Another significant observation was that at La Sima the CO_2 fluxes in the CO_2 -rich gas emission sites were higher than those recorded along the Jabalón River, with the exception of the water-degassing points, whereas the ^{222}Rn activities showed an opposite behavior. At La Sima the highest CO_2 fluxes were from 3000 to 5000 g·m⁻²·d⁻¹ and the ^{222}Rn concentrations were clustering

around 120 kBq m⁻³ (Table 1; #1, #8 a#24). Conversely, at Jabalón River the CO_2 flux was 200 g·m⁻²·d⁻¹ (e.g., #18 and #59) and the ^{222}Rn concentration was around 400 kBq m⁻³ (e.g., #18 and #62). This would support the hypothesis that along the Jabalón River a radon source derived from dissolved U and Ra adds to that

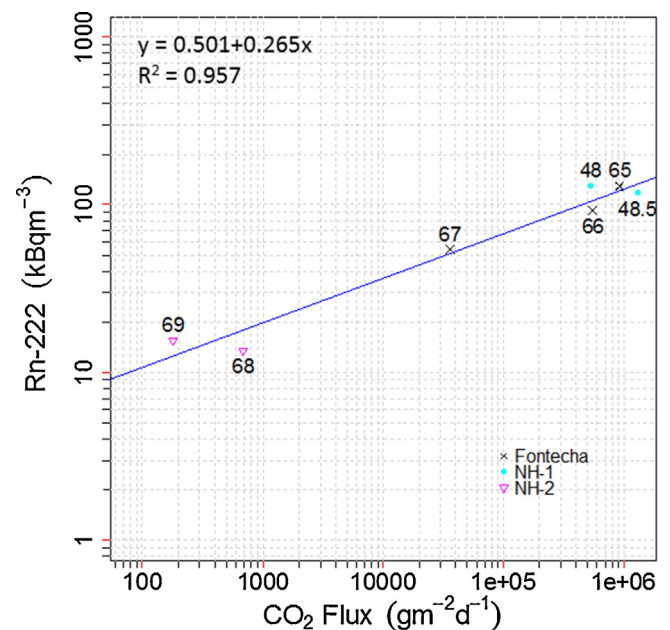


Fig. 11. Correlation between CO_2 flux and ^{222}Rn in the degassing pools (Table 2, Fig. 3).

transported by CO₂. While at La Sima the only cause that leads to the increase in radon is the CO₂ flux, in the Jabalon River contributions from soil water, U and Ra and CO₂ flux are to be added. Thus, this would explain why at La Sima we measured high CO₂ fluxes while the ²²²Rn activities were relatively lower than that in the Jabalon River area.

5.3. Implication for monitoring CO₂ storage sites

The CO₂-rich emissions at CCVF are mainly associated with fracture systems and the gas discharges are regarded as point-source seepage, being occasionally characterized by relatively high flow: 1 t m⁻² d⁻¹ or even higher. In the vicinity of these sites, the CO₂ fluxes approach values, which are typical of soil respiration. In the perspective of assessing gas leakages in areas selected for geological carbon storage, the observation of the point-source seepage reveals that the detection of leakage sites can pose serious difficulties given the large area potentially affected by the leakage of injected CO₂ (hundreds km²). It is worth mentioning that the amount of CO₂ emitted from these points can be of the order of magnitude of the maximum leakage rate considered acceptable (0.1% of the total amount in storage per year; Van der Zwaan and Smekens, 2006) for a commercial storage project (i.e., approximately 1 Mt year⁻¹; such as in Snohvit: 0.73 Mt year⁻¹, Sleipner: 0.98 Mt year⁻¹ and In Salah: 1.28 Mt year⁻¹; Michael et al., 2010). Thus, conventional approaches might not be able to detect small-scale emissions.

In this regards, in the framework of CCS projects significant variations in terms of soil diffuse CO₂ flux may be occurring at the scale of few meters or even centimeters and CO₂ leakages cannot be detected until clear evidences (e.g., impacts on the vegetation, newly formed bubbling sites) are visible in the field, even when small sample grids, e.g., 10–20 m (e.g., Elío et al., 2013 and references therein) are considered. Besides, natural analogs (e.g., geothermal or volcanic areas) have gas fluxes, which are by far higher than those expected for a sequestration project. Furthermore, in the case of seepages small geographic changes and moderate seasonal changes in the CO₂ fluxes are expected to be detected with respect to the background levels. This makes the reconnaissance of seepages real challenging.

The application of other cost-effective monitoring/detection techniques able to cover larger areas, such as Eddy covariance, open-path laser and remote sensing, need to be improved and properly evaluated for their applicability to CCS projects (e.g., Klusman, 2011; Lewicki et al., 2009; Ortega et al., 2014). Long-term continuous soil gas surveys can help to identify leakages (e.g., Schlömer et al., 2014), although these might also be undetectable when occurring in very localized and small areas.

Concerning radon measurements in the CCVF areas, an increase in the ²²²Rn soil-gas concentration was detected and correlated to the CO₂ flux. The influence of this ²²²Rn anomaly zone, though small, seems to be of larger extent with respect to that of CO₂. Consequently, radon isotopes can be considered as good tracers to discriminate leakage areas, providing useful information about the (biological or deep-seated) origin of CO₂. Radon isotope measurements can overcome the limitations of others geochemical methods, which are commonly used to interpret the origin of the soil gases, e.g., δ¹³C–CO₂ or helium isotope ratios. Another advantage of radon measurements is that to avoid “false positives”. Radon activity in soil-gas is indeed related to lithological and geostructural (faults and fractures) features. This means that when an increase “deep” CO₂ fluxes with respect to the background values occurs, radon activity is also expected to increment. Conversely, if CO₂ fluxes increase in response of an enhanced biological activity, radon activity should not suffer any particular variation.

At CCVF, the ²²²Rn activity in the soil gas was occasionally as high as 430 kBq m⁻³, i.e., much higher than the threshold value

(>50 kBq m⁻³; Cothorn and Smith, 1987) for which a certain site is considered with a high-risk potential. Such high concentrations need to be taken into account when CCS risk assessment plans are to be designed, particularly when CO₂ leakages may affect residential areas and working environments. Consumption of CO₂-rich waters is also a risk since they may potentially contain high concentrations of dissolved ²²²Rn, and U and Ra.

In this study, correlations between ²²⁰Rn concentrations and CO₂ fluxes were not as clear as observed for those of ²²²Rn and CO₂. In the dry gas vent of La Sima, a significant reduction of the ²²⁰Rn concentrations was detected and likely related to an increase in the CO₂ flux. However, in the emission sites associated with water springs ²²²Rn and CO₂ were not correlated while a slight increase in ²²⁰Rn concentrations with the CO₂ flux was recorded. This effect is likely due to different source of ²²²Rn and ²²⁰Rn isotopes.

6. Conclusions

The Campo de Calatrava Volcanic Field is a relevant natural analog where gas leakages in the framework of geological CO₂ storage projects can be investigated. A large number of CO₂-rich emissions, predominantly associated with fracture/fault systems occur, although they mainly discharge as punctual manifestations. The results suggest a deep origin of CO₂, in agreement with previous geochemical and isotopic analyses of the gas leaks, which indicate that CO₂ is mantle sourced.

According to our data, the increase of ²²²Rn in the soil gases is likely produced by two mechanisms, (i) advective transport where CO₂ acts as carrier gas and (ii) generation at shallow level due to the presence of U and Ra in both thermal waters and soils.

Geochemical surveys of CO₂ flux and radon isotopic measurements are very useful to: (i) define and quantify CO₂ leakages once detected and (ii) monitor the evolution of the leakages and the effectiveness of subsequent remediation activities. These techniques can also be successfully applied to detect diffuse leakages.

Acknowledgements

We wish to thank C. Jenkins and Nunzia Voltattorni and an anonymous reviewer who greatly improved an early version of the manuscript. This work was funded by the Ciudad de la Energía Foundation (CIUDEN), through the ALM-08-006 contract, and co-financed by the European Union (European Energy Programme for Recovery). The sole responsibility of this publication lies with the authors. The European Union is not responsible for any use that may be made of the information contained therein.

References

- Ancochea, E., (Ph.D. thesis) 1983. *Evolución espacial y temporal del volcanismo reciente de España Central*. Complutense University, Madrid.
- Bonotto, D.M., Andrews, J.N., 1999. Transfer of radon and parent nuclides ²³⁸U and ²³⁴U from soils of the Mendip Hills area, England, to the water phase. *J. Geochem. Explor.* 66, 255–268.
- Cardellini, C., Chiodini, G., Frondini, F., 2003. Application of stochastic simulation to CO₂ flux from soil: mapping and quantification of gas release. *J. Geophys. Res.* 108 (B9), 2425.
- Casas, I., de Pablo, J., Gimenez, J., Torrero, M.E., Bruno, J., Cera, E., Finch, R.J., Ewing, R.C., 1998. The role of pe, pH, and carbonate on the solubility of UO₂ and uraninite under nominally reducing conditions. *Geochim. Cosmochim. Acta* 62 (13), 2223–2231.
- Cebriá, J.M., López-Ruiz, J., Carmona, J., Doblas, M., 2009. Quantitative petrogenetic constraints on the Pliocene alkali basaltic volcanism of the SE Spain Volcanic Province. *J. Volcanol. Geoth. Res.* 185, 172–180.
- Cebriá, J.M., López-Ruiz, J., 1995. Alkali basalts and leucites in an extensional intra-continental plate setting: the Late Cenozoic Calatrava Volcanic Province (Central Spain). *Lithos* 35, 27–46.
- Chiodini, G., Cioni, R., Guidi, M., Raco, B., Marini, L., 1998. Soil CO₂ flux measurements in volcanic and geothermal areas. *Appl. Geochem.* 13 (5), 543–552.
- Cothorn, R.C., Smith, J.E., 1987. *Environmental Radon*. Environmental Science Research, vol. 35. Plenum Press, New York.

- Cox, M.E., 1980. Ground radon surveys of a geothermal area in Hawaii. *Geophys. Res. Lett.* 7, 283–286.
- Crespo, A., (Ph.D. thesis) 1992. *Geología, mineralogía y génesis de los yacimientos de manganeso cobaltífero del Campo de Calatrava (Ciudad Real)*. UCM, pp. 389.
- Davis, B.M., Istok, J.D., Semprini, L., 2003. Static and push-pull methods using radon-222 to characterize dense nonaqueous phase liquid. *Groundwater* 41, 470–481.
- De Jong, E., Acton, D.F., Kozak, L.M., 1994. Naturally occurring gamma-emitting isotopes, radon release and properties of parent materials of Saskatchewan soils. *Can. J. Soil Science* 74, 47–53.
- Dueñas, B.C., Fernández, M.C., 1987. Dependence of radon-222 flux on concentrations of soil gas and análisis of the effects produced by several atmospheric variables. *Ann. Geophys.* 79, 5025–5029.
- Elío, J., Nisi, B., Ortega, M.F., Mazadiego, L.F., Vaselli, O., Grandía, F., 2013. CO₂ soil flux baseline at the CO₂ Injection pilot Plant of Hontomin (Burgos, Spain). *Int. J. Greenh. Gas Control* 18, 224–236.
- EPA, US, 2003. *EPA Assessment of Risks from Radon in Homes*. Office of Radiation and Indoor Air, United States Environmental Protection Agency, Washington, DC.
- Etiopie, G., Martinelli, G., 2002. Migration of carrier and trace gases in the geosphere: an overview. *Phys. Earth Planet. In.* 129, 185–204.
- Etiopie, G., Guerra, M., Raschi, A., 2005. Carbon dioxide and radon geohazards over a gas-bearing fault in the Siena graben (Central Italy). *Terr. Atmos. Ocean Sci.* 16 (4), 885–896.
- Field, R.W., Steck, D.J., Smith, B.J., Brus, C.P., Fisher, E.L., Neuberger, J.S., Platz, C.E., Robinson, R.A., Woolson, R.W., Lynch, F., 2000. Residential radon gas exposure and lung cancer. The Iowa radon lung cancer study. *Am. J. Epidemiol.* 151 (11), 1091–1102.
- Fleischer, R.L., 1997. Radon: overview of properties, origin and transport. In: Durrani, S.A., Ilic, R. (Eds.), *Radon Measurements by Etched Track Detectors, Applications in Radiation Protection, Earth Sciences and the Environment*. World Scientific, Singapore, pp. 1–20.
- Fleischer, R.L., Mogro-Campero, A., 1978. Mapping of integrated radon emanation for detection of long-distance migration of gases within the earth: techniques and principles. *J. Geophys. Res.* 83 (B7), 3539–3549.
- Gal, F., Brach, M., Braibant, G., Bény, C., Michel, K., 2012. What can be learned from natural analogue studies in view of CO₂ leakage issues in Carbon Capture and Storage applications? Geochemical case study of Sainte-Marguerite area (French Massif Central). *Int. J. Greenh. Gas Control* 10, 470–485.
- García-González, J.E., Ortega, M.F., Chacón, E., Mazadiego, L.F., De Miguel, E., 2008. Field validation of radon monitoring as a screening methodology for NAPL-contaminated sites. *Appl. Geochem.* 23, 2753–2758.
- Giammanco, S., Sims, K.W.W., Neri, M., 2007. Measurements of ²²⁰Rn and ²²²Rn and CO₂ emissions in soil and fumarole gases on Mt. Etna volcano (Italy): implications for gas transport and shallow ground fracture. *Geochim. Geophys. Geosyst.* 8 (10), 1–14.
- Gorman-Lewis, D., Burns, P., Fein, J.B., 2008. Review of uranyl mineral solubility measurements. *J. Chem. Thermodyn.* 40, 335–352.
- Guerra, M., Lombardi, S., 2001. Soil-gas method for tracing neotectonic faults in clay basins: the Pisticci field (Southern Italy). *Tectonophysics* 339, 511–522.
- Hernández-Pacheco, F., 1932. Estudio de la región volcánica central de España. *Mem. R. Acad. Cienc. Exactas Fis. Nat. Madr., Ser. Cienc. Nat.* 3, 1–235.
- Holloway, S., Pearce, J.M., Hards, V.L., Ohsumi, T., Gale, J., 2007. Natural emissions of CO₂ from the geosphere and their bearing on the geological storage of carbon dioxide. *Energy* 32, 1194–1201.
- Hsi, C.K.D., Langmuir, D., 1985. Adsorption of uranyl onto ferric oxyhydroxides: application of the surface complexation site-binding model. *Geochim. Cosmochim. Acta* 49, 1931–1941.
- Huxol, S., Brennwald, M.S., Hoehn, E., Kipfer, R., 2012. On the fate of ²²⁰Rn in soil material in dependence of water content: implications from field and laboratory experiments. *Chem. Geol.* 298–299, 116–122.
- Huxol, S., Brennwald, M.S., Kipfer, R., 2013. Processes controlling ²²⁰Rn concentrations in the gas and water phases of porous media. *Chem. Geol.* 335, 87–92.
- IEA, 2008. *Energy Technology Perspectives*. OECD/IEA, Paris.
- IGME, 1988. *Mapa Geológico de España E: 1:50.000. Hoja n.º 784, Ciudad Real*. I.G.M.E., Madrid.
- Ioannides, K., Papachristodoulou, C., Stamoulis, K., Karamanis, D., Pavlides, S., Chatzipetros, A., Karakala, E., 2003. Soil gas radon: a tool for exploring active fault zones. *Appl. Radiat. Isot.* 59, 205–213.
- IPCC, 2005. In: Metz, B., Davidson, O., de Coninck, H.C., Loos, M., Meyer, L.A. (Eds.), *IPCC Special Report on Carbon Dioxide Capture and Storage*. Prepared by Working Group III of the Intergovernmental Panel on Climate Change. Cambridge University Press, Cambridge/United Kingdom/New York, NY, USA, p. 442.
- IPCC, 2006. In: *National Greenhouse Gas Inventories Programme*, Eggleston, H.S., Buendia, L., Miwa, K., Ngara, T., Tanabe, K. (Eds.), *Guidelines for National Greenhouse Gas Inventories*. IGES, Japan.
- Jeandel, E., Battani, A., Sarda, P., 2010. Lessons learned from natural and industrial analogues for storage of carbon dioxide. *Int. J. Greenh. Gas Control* 4, 890–909.
- King, C.Y., Minissale, A., 1994. Seasonal variability of soil-gas radon concentration in central California. *Radiat. Meas.* 23, 683–692.
- Klusman, R., Voorhees, K.J., 1983. A new development in petroleum exploration technology. *Mines Mag.* 73, 121–149.
- Klusman, R.W., 2011. Comparison of surface and near-surface geochemical methods for detection of gas microseepage from carbon dioxide sequestration. *Int. J. Greenh. Gas Control* 5, 1369–1392.
- Kühn, M., Busch, A., Niemi, A., Amann-Hildenbrand, A., 2013. Preface: CO₂ storage is feasible and further demonstration projects are needed. CO₂ storage at the EGU general assembly 2012. *Int. J. Greenh. Gas Control* 19, 606–608.
- Langmuir, D., 1978. Uranium solution-mineral equilibria at low temperatures with applications to sedimentary ore deposits. *Geochim. Cosmochim. Acta* 42, 547–569.
- Langmuir, D., Melchior, D., 1985. The geochemistry of Ca, Sr, Ba and Ra sulfates in some deep brines from the Palo Duro Basin, Texas. *Geochim. Cosmochim. Acta* 49, 2423–2432.
- Langmuir, D., Riese, A.C., 1985. The thermodynamic properties of radium. *Geochim. Cosmochim. Acta* 49, 1593–1601.
- Lewicki, J., Hilley, G., Fischer, M., Pan, L., Curtis, O., Dobeck, L., Spangler, L., 2009. Detection of CO₂ leakage by eddy covariance during the ZERT project's CO₂ release experiments. *Energy Procedia* 1, 2301–2306.
- Lewicki, J., Birkholzer, J., Tsang, C.F., 2007. Natural and industrial analogues for leakage of CO₂ from storage reservoirs: identification of features, events, and processes and lessons learned. *Environ. Geol.* 52 (3), 457–467.
- López-Ruiz, J., Cebriá, J.M., Doblas, M., 2002. Cenozoic volcanism I: the Iberian Peninsula. In: Gibbons, W., Moreno, T. (Eds.), *The Geology of Spain*. Geological Society, London, pp. 417–438.
- Lupion, M., Herzog, H.J., 2013. NER300: lessons learnt in attempting to secure CCS projects in Europe. *Int. J. Greenh. Gas Control* 19, 19–25.
- Majumdar, D., Roszak, S., Balasubramanian, K., Nitsche, H., 2003. Theoretical study of aqueous uranyl carbonate (UO₂CO₃) and its hydrated complexes: UO₂CO₃·nH₂O (n = 1–3). *Chem. Phys. Lett.* 372, 232–241.
- Martin, P., Akber, R.A., 1999. Radium isotopes as indicators of adsorption-desorption interactions and barite formation in groundwater. *J. Environ. Radioact.* 46, 271–286.
- Martinelli, G., 1998. Gas geochemistry and ²²²Rn migration processes. *Radiat. Prot. Dosim.* 78 (1), 77–82.
- Mazadiego, L.F., (Ph.D. thesis) 1994. *Desarrollo de una metodología para la prospección geoquímica en superficie de combustibles fósiles*. Polytechnic University of Madrid.
- Melero Cabañas, D., 2007. *Ciudad Real: tierra de hervideros, fuentes y baños de aguas minero-medicinales*. Imprenta Provincial, Ciudad Real, pp. 254.
- Michael, K., Golab, A., Shulakova, V., Ennis-King, J., Allinson, G., Sharma, S., Aiken, T., 2010. Geological storage of CO₂ in saline aquifers—a review of the experience from existing storage operations. *Int. J. Greenh. Gas Control* 4, 659–667.
- Michel-Le Piesres, K., Gal, F., Brach, M., Guignat, S., 2010. Radon, helium and CO₂ measurements in soils overlying a former exploited oilfield, Pechelbronn district, Bas-Rhin, France. *J. Environ. Radioact.* 10, 835–846.
- Morse, J.G., Rana, M.H., Morse, L., 1982. Radon mapping as indicators of subsurface oil and gas. *Oil Gas J.* 80, 227–246.
- Nance, H.S., Rauch, H., Strazisar, B., Bromhal, G., Wells, A., Diehl, R., Klusman, R., Lewicki, J., Oldenburg, C., Kharaka, Y.K., Kakouros, E., 2005. Surface environmental monitoring at the Frio CO₂ sequestration test site, Texas. In: *National Energy Technology Laboratory Fourth Annual Conference on Carbon Capture and Sequestration*, Alexandria, VA, May 2–5, GCCC Digital Publication Series #05-04, pp. 1–16.
- Nazaroff, W.W., Nero Jr., A.V., 1988. *Radon and Its Decay Products in Indoor Air*. John Wiley & Sons, United States of America.
- Nataly Echevarria Huaman, R., Xiu Jun, T., 2014. Energy related CO₂ emissions and the progress on CCS projects: a review. *Renew. Sustain. Energy Rev.* 31, 368–385.
- NETL, DOE/NETL-311/081508 2009. *Best Practices For: Monitoring, Verification, and Accounting of CO₂ Stored in Deep Geologic Formations*. National Energy Technology Laboratory.
- Nielson, D.L., IDO/78-1701.b.1.1.2 1978. *Radon Emanometry as a Geothermal Exploration Technique: Theory and an Example from Roosevelt Hot Springs KGRA*. University of Utah Research Institute, Earth Science Laboratory, Utah, Salt Lake City.
- Oldenburg, C.M., 2003. Carbon dioxide as cushion gas for natural gas storage. *Energy Fuels* 17, 240–246.
- Oldenburg, C.M., 2012. Why we need the 'and' in 'CO₂ utilization and storage'. *Greenh. Gas Sci. Technol.* 2, 1–2, <http://dx.doi.org/10.1002/ghg.1274>.
- Ortega, M.F., Rincones, M., Elío, J., Gutiérrez del Olmo, J., Nisi, B., Mazadiego, L.F., Iglesias, L., Vaselli, O., Grandía, F., García, R., De la Vega, R., Llamas, B., 2014. Gas monitoring methodology and application to CCS projects as defined by atmospheric and remote sensing survey in the natural analogue of Campo de Calatrava. *Global NEST J.* 16 (2), 269–279.
- Pearce, J.M., 2006. What can we learn from natural analogues? In: Lombardi, S., Altunina, L.K., Beaubien, S.E. (Eds.), *Advances in the Geological Storage of Carbon Dioxide*. Springer, Netherlands, pp. 129–140.
- Pérez, N.M., Nakai, S., Wakita, H., Albert-Bertan, J.F., Redondo, R., 1996. Preliminary results on the ³He/⁴He isotopic ratios in terrestrial fluids from Iberian Peninsula: seismotectonic and neotectonic implications. *Geogaceta* 20, 830–833.
- Piedrabuena, M.A.P., 1992. *Las última manifestaciones asociadas al vulcanismo del Campo de Calatrava (Ciudad Real): los manantiales termales*. Cuadernos de Sección Historia 20, 187–201.
- Quindós, L.S., Sainz, C., Fuente, I., Nicolás, J., Quindós, L., Arteché, J., 2006. Correction by self-attenuation in gamma-ray spectrometry for environmental samples. *J. Radioanal. Nucl. Chem.* 270 (2), 339–343.
- Ramachandran, T.V., Sathish, L.A., 2011. Nationwide indoor ²²²Rn and ²²⁰Rn map for India: a review. *J. Environ. Radioact.* 102, 975–986.
- Riding, J.B., Rochelle, C.A., 2005. *The IEA Weyburn CO₂ Monitoring and Storage Project*. Final Report of the European Research Team. British Geological Survey Research Report, RR/05/03., pp. 54.

- Romanak, K., Harmon, R., Kharaka, Y., 2013. Editorial: geochemical aspects of geologic carbon storage. *Appl. Geochem.* 30, 1–3.
- Rosario, A.S., Wichmann, H.-E., 2006. Environmental pollutants: radon. In: *Encyclopedia of Respiratory Medicine*, pp. 120–125.
- Rose, A.W., Hawkes, H.E., Webb, J.S., 1979. *Geochemistry in mineral exploration*, 2nd ed. Academic Press.
- Schlömer, S., Möller, I., Furch, M., 2014. Baseline soil gas measurements as part of a monitoring concept above a projected CO₂ injection formation—a case study from Northern Germany. *Int. J. Greenh. Gas Control* 20, 57–72.
- Schubert, M., Freyer, K., Treutler, H.C., Weitb, H., 2001. Using the soil gas radon as an indicator for ground contamination by non-aqueous phase-liquids. *J. Soils Sediments* 1 (4), 217–222.
- Solomon, S., Carpenter, M., Flach, T.A., 2008. Intermediate storage of carbon dioxide in geological formations: a technical perspective. *Int. J. Greenh. Gas Control* 2, 502–510.
- Strutt, M.H., Beaubien, S.E., Beaubron, J.C., Brach, M., Cardellini, C., Granieri, R., Jones, D.G., Lombardi, S., Penner, L., Quattrocchi, F., Voltattorni, N., 2003. Soil gas as a monitoring tool of deep geological sequestration of carbon dioxide: preliminary results from the Encana EOR Project in Weyburn, Saskatchewan (Canada). *Greenh. Gas Control Technol.* 1, 391–395.
- Sutton, W., Soonwala N., 1975. A Soil Radium Method for Uranium Prospecting. *Mineral Exploration* 5.
- Szabó, K.Z., Jordan, G., Horváth, Á., Szabó, Cs., 2013. Dynamics of soil gas radon concentration in a highly permeable soil based on a long-term high temporal resolution observation series. *J. Environ. Radioact.* 124, 74–83.
- Tanner, A.B., 1980. Radon migration in the ground: supplementary review. In: Gesell, T.F., Lowder, W.M. (Eds.), *Proc. Natural Radiation Environment III, Conf.-780422*. US Dept. of Commerce, National Technical Information Service, Springfield, VA, p. 5.
- Toutain, J.P., Baubron, J.C., 1999. Gas geochemistry and seismotectonics: a review. *Tectonophysics* 304, 1–27.
- UNFCCC, 2011. Conference of the Parties Serving as the Meeting of the Parties to the Kyoto Protocol. FCCC/KP/CMP/20017L.4. United Nations Framework Convention on Climate Change (UNFCCC), Durban.
- Van der Zwaan, B., Smekens, K., 2006. CO₂ capture and storage with leakage in an energy-climate model. *Environ. Model. Assess.* 14 (2), 135–148.
- Vaselli, O., Nisi, B., Tassi, F., Giannini, L., Grandia, F., Darrah, T., Capecchiacci, F., Perez del Villar, L., 2013. Water and gas geochemistry of the Calatrava Volcanic Province (CVP) hydrothermal system (Ciudad Real, Central Spain). *Geophysical Research Abstracts*, 10th EGU General Assembly, EGU2013-11102.
- Vaupotic, J., Barisic, D., Kobal, I., Lulic, S., 2007. Radioactivity and radon potential of the terra rossa soil. *Radiat. Meas.* 42, 290–297.
- Virk, H.S., Walia, V., 2001. Helium/radon precursory signals of Chamoli Earthquake, India. *Radiat. Meas.* 34, 379–384.
- Voltattorni, N., Sciarra, A., Caramanna, G., Cinti, D., Pizzino, L., Quattrocchi, F., 2009. Gas geochemistry of natural analogues for the studies of geological CO₂ sequestration. *Appl. Geochem.* 24, 1339–1346.
- Walia, V., Lin, S.J., Fu, C.C., Yang, T.F., Hong, W., Wen, K., Chen, C., 2010. Soil-gas monitoring: a tool for fault delineation studies along Hsinhua Fault (Tainan), Southern Taiwan. *Appl. Geochem.* 25, 602–607.
- Wilson, M., Monea, M., 2004. IEA GHG Weyburn CO₂ monitoring and storage project, summary report 2000–2004. In: *Proceedings of the 7th International Conference on Greenhouse Gas Control Technologies*, Petroleum Technology Research Centre, Vancouver, Canada.
- Yu, C., Loureiro, C., Cheng, J.-J., Jones, L.G., Wang, Y.Y., Chia, Y.P., Faillace, E., 1993. Data Collection Handbook to Support Modeling Impacts of Radioactive Materials in Soil. Environmental Assessment and Information Sciences Division, Argonne National Laboratory, Argonne, IL.